INORGANIC CHEMISTRY
FRONTIERS

RESEARCH ARTICLE

View Article Online
View Journal | View Issue

Cite this: *Inorg. Chem. Front.*, 2023, **10**, 6746

Site occupation and upconversion process enabled multicolor emission in a $Gd_3GaO_6:Bi^{3+}$, Er^{3+} phosphor for quad-mode anti-counterfeiting†

Zhijun Li,[a,b] Zeyu Lyu,*[a] Pengcheng Luo,[a,b] Shuai Wei,[a,b] Chengyu Zhuo,[a,b] Dashuai Sun,[a] Sida Shen[a] and Hongpeng You *[a,b,c]

The development of multicolor emissions in a single phosphor poses a significant challenge with practical implications for high-security-level multi-mode anti-counterfeiting. Herein, a novel $Gd_3GaO_6:Bi^{3+},Er^{3+}$ phosphor with multicolor emissions was successfully prepared and its structural and luminescence properties were investigated. In Bi^{3+}-doped phosphors, the Bi^{3+} ions occupy two different Gd^{3+} sites and exhibit blue-violet light at 409 nm and orange emission at 594 nm, respectively. Besides, Er^{3+}-doped phosphors show green downshifting luminescence under the excitation of 378 nm, green upconversion luminescence under the excitation of 980 nm, and yellow upconversion luminescence under the excitation of 1530 nm. The $Gd_3GaO_6:Bi^{3+},Er^{3+}$ phosphor displays the emissions of both Bi^{3+} and Er^{3+} under the specific excitation wavelengths. On this basis, a quad-mode anti-counterfeiting material with high security levels has been designed and manufactured, and different luminescence patterns can be obtained under the excitations of 302, 365, 980 and 1530 nm. This work not only presents a well-performing phosphor for advanced anti-counterfeiting, but also paves the way for designing multicolor emission in one phosphor.

Received 3rd August 2023,
Accepted 27th September 2023

DOI: 10.1039/d3qi01525d

rsc.li/frontiers-inorganic

1. Introduction

Nowadays, anti-counterfeiting plays a significant role in the fields of banknotes, pharmaceuticals, confidential documents, jewelry, identity cards, and so on.[1–4] Generally, anti-counterfeiting labels should meet several criteria, including being low-cost, mass-produced, chemically stable, environmentally friendly, difficult to replicate, and easily identifiable using simple and portable devices. Based on these considerations, anti-counterfeiting patterns, painted with "security inks" based on luminescent materials, have attracted enormous attention.[5] These security inks are typically prepared by adding luminescent materials to matrices (such as suspensions containing solvents, surfactants, polymers or other additives).[6] The reliability of anti-counterfeiting is largely dependent on the performance of the added luminescent materials. The materials with multicolor emission, either the excitation orthogonalized emissions[7,8] or different emissions in the localized parts of a single microcrystal,[9,10] can offer highly distinguishable patterns for multi-mode anti-counterfeiting with a higher security level.[11]

Compared with other types of luminescent materials such as organic dyes, quantum dots and metal complexes, ion-doped inorganic materials offer a distinct advantage of readily realizing multicolor emission.[12,13] In some phosphors involving an energy transfer process, emission color can be changed by varying the ratio of the donor and acceptor ions.[14,15] For example, the downshifting (DS) emission in some phosphors can be adjusted from reddish to greenish through changing the dopant from Eu^{3+} to Tb^{3+} ions.[8] In order to construct multi-mode anti-counterfeiting materials, it is usually necessary to synthesize several phosphors with different colors separately. It is more convenient and practical to realize multicolor emissions in just one luminescent material. As we are aware, Bi^{3+} is an efficient non-rare earth activator, and its exposed s–p electrons make the emission behavior highly sensitive to the crystal field.[16] Actually, Bi^{3+} can emit distinguishable colors under different excitation wavelengths when it locates at different crystal sites of the host.[17–19]

[a]*Key Laboratory of Rare Earths, Chinese Academy of Sciences; Ganjiang Innovation Academy, Chinese Academy of Sciences, Ganzhou 341000, P.R. China. E-mail: hpyou@ciac.ac.cn, zylyu@gia.cas.cn*
[b]*School of Chemistry and Chemical Engineering, Nanchang University, Nanchang 330031, P.R. China*
[c]*State Key Laboratory of Rare Earth Resource Utilization, Changchun Institute of Applied Chemistry, Chinese Academy of Sciences, Changchun 130022, P. R. China*
† Electronic supplementary information (ESI) available. See DOI: https://doi.org/10.1039/d3qi01525d

In addition, lanthanide-doped materials with upconversion (UC) emission modes, which require a specific excitation wavelength, have been demonstrated to have potential applications in high-security-level anti-counterfeiting and have attracted extensive interest.[20–22] In some UC processes, the excitation can effectively control the emission.[8] Therefore, we reason that the combination of the DS emission from Bi^{3+} and the UC emission from lanthanide ions, such as Er^{3+}, can potentially achieve multi-mode anti-counterfeiting in a single phosphor.

Herein, we design a novel Bi^{3+} and Er^{3+} codoped gallium oxide phosphor Gd_3GaO_6:Bi^{3+},Er^{3+} (abbreviated as GGO:Bi^{3+}, Er^{3+}). The crystal structure demonstrates that there are two doping sites of Bi^{3+} ions in the Gd_3GaO_6 host, leading to excitation orthogonalized purple and orange emissions. Besides, these materials are able to achieve green and yellow UC luminescence under 980 or 1530 nm near-infrared laser excitation, respectively. Finally, they are applied to anti-counterfeiting patterns by mixing them with ink to produce security inks, and quad-mode anti-counterfeiting is achieved. The results indicate that Gd_3GaO_6:Bi^{3+},Er^{3+} is a potential luminescent material for information encryption and anti-counterfeiting applications.

2. Experimental

2.1. Materials and synthesis

A series of Gd_3GaO_6:Bi^{3+}/Er^{3+} samples were synthesized by the traditional solid-state reaction method. The stoichiometric mixtures of Gd_2O_3 (99.99%), Ga_2O_3 (99.99%), Bi_2O_3 (99.99%) and Er_2O_3 (99.99%) were ground in an agate mortar and filled into an alumina crucible. The raw materials were sintered at 1350 °C for 5 h. After that, the obtained samples were cooled down to room temperature in the furnace, and finely ground for further characterization.

2.2. Characterization

Powder X-ray diffraction (XRD) measurements were performed on a D8 Advance diffractometer (Bruker Corporation, Germany) at 40 kV and 40 mA with Cu Kα radiation (λ = 1.5406 Å). SEM images were obtained on a field emission scanning electron microscope (JSM-IT800, JEOL) and the elemental composition was analyzed using an energy-dispersive spectrometer (Oxford Instruments) coupled to an electron microscope. Photoluminescence excitation (PLE) and emission (PL) spectra were obtained with a Hitachi F-7100 spectrophotometer equipped with a 150 W xenon lamp and a 980/1530 nm laser as the excitation source. The fluorescence decay curves were obtained from an Edinburgh FLS1000 spectrometer. The temperature-dependent (25–210 °C) spectra were obtained using an Everfine EX-1000 excitation spectra and thermal quenching analyzer for phosphors.

3. Results and discussion

3.1. Phase identification and crystal structure

To analyze the phase purity, the XRD patterns of Gd_3GaO_6:xBi^{3+} (x = 0.03, 0.05, 0.09, 0.12) and Gd_3GaO_6:0.05Bi^{3+},0.04Er^{3+} samples and the standard data card (PDF 53-1225) are presented in Fig. 1a. The diffraction peaks of the samples are in good agreement with the index card and there are no extra diffraction peaks, verifying that the Bi^{3+} and Er^{3+} ions are completely doped into the host lattice. Fig. 1b depicts the crystal structure of GGO. The GGO host belongs to the orthorhombic unit cell with the space group $Cmc2_1$. There are three different cationic sites in the host lattice, including two Gd^{3+} sites and

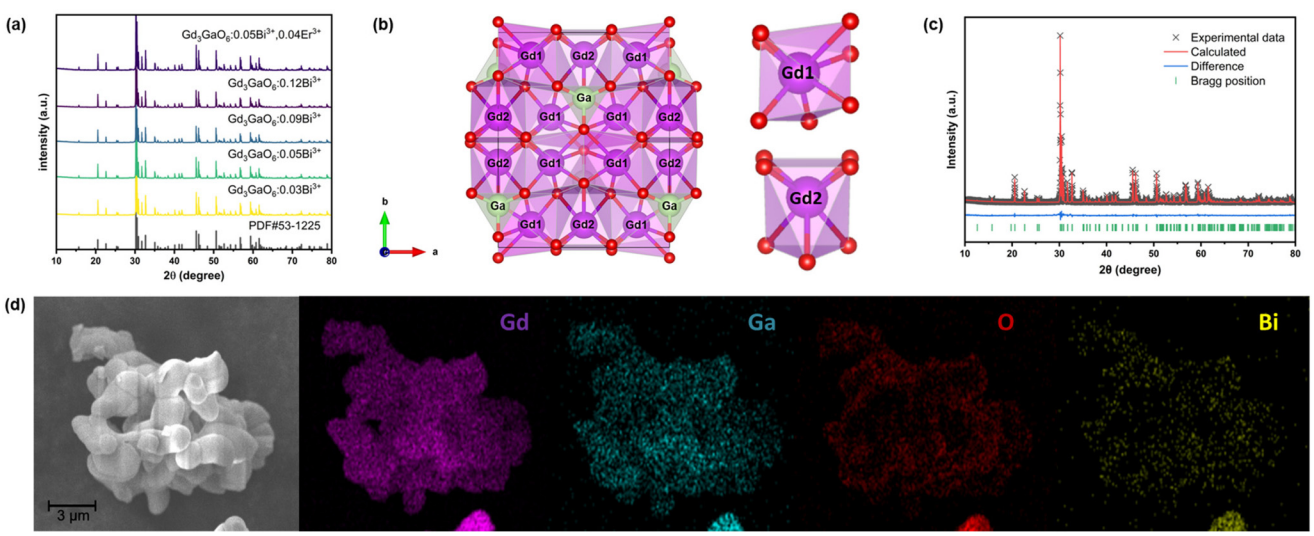

Fig. 1 (a) XRD patterns of the obtained phosphors and the standard card of the host (PDF #53-1225). (b) Crystal structure of GGO and the coordination environment of Gd^{3+}. (c) Rietveld refinement of the XRD pattern of GGO:0.09Bi^{3+}. (d) SEM image of the phosphor and element mapping images of Gd, Ga, O and Bi.

one Ga^{3+} site. The two Gd^{3+} ions are at the center of a decahedron [GdO_7] coordinated by seven oxygen atoms, and Ga^{3+} is surrounded by four oxygen atoms to form a tetrahedron [GaO_4]. Considering the radius and valence state of the ions, the Bi^{3+} and Er^{3+} ions replace the Gd^{3+} ions.

Rietveld refinements of GGO:0.09Bi^{3+} and GGO:0.05Bi^{3+},0.04Er^{3+} were performed using the general structure analysis system (GSAS) program. Fig. 1c and S1† show the experimental and calculated results for the Rietveld refinements of these two samples, with the single crystal data of Gd_3GaO_6 (ICSD 280077) used as the original reference. The detailed Rietveld refinement results and cell parameters are illustrated in Table 1, where the low residual factors further indicate that the phosphors obtained are pure in phase. Besides, the refinement results of GGO:$x$$Bi^{3+}$ (x = 0.03–0.12) are illustrated in Table S1 and Fig. S2.† As the concentration of Bi^{3+} ions increases, there is a clear tendency for the lattice parameters to increase. This can be attributed to the larger radius of the Bi^{3+} ion than that of the substituted Gd^{3+} ion. Fig. 1d shows the SEM image of GGO:0.07Bi^{3+}, and the elemental mapping indicates that the Gd, Ga, O, and Bi elements are clearly and uniformly distributed.

Table 1 Rietveld refinement results and crystal data for GGO:0.09Bi^{3+} and GGO:0.05Bi^{3+},0.04Er^{3+}

Sample	GGO:0.09Bi^{3+}	GGO:0.05Bi^{3+},0.04Er^{3+}
Symmetry	Orthorhombic	Orthorhombic
Space group	$Cmc2_1$ (no. 36)	$Cmc2_1$ (no. 36)
Cell parameters	a = 8.9994 Å, b = 11.2846 Å, c = 5.4836 Å, $\alpha = \beta = \gamma$ = 90°, V = 556.885 Å^3	a = 8.9952 Å, b = 11.2814 Å, c = 5.4820 Å, $\alpha = \beta = \gamma$ = 90°, V = 556.305 Å^3
Reliability factors	χ^2 = 2.246, R_{wp} = 7.22%, R_p = 5.99%	χ^2 = 3.137, R_{wp} = 9.14%, R_p = 7.83%

3.2. Photoluminescence of GGO:Bi^{3+} phosphors

Fig. 2a shows the PLE and PL spectra of GGO:0.07Bi^{3+}. Under the excitation of 296 nm, the PL spectrum ranges from 350 to 500 nm with a maximum at 409 nm. And the PLE spectrum monitored at 409 nm shows a broad band in the range of 200–350 nm peaking at 296 nm. Additionally, when excited at 375 nm, the sample shows orange emission, and the peak position of the emission band is at about 594 nm. The corresponding PLE spectrum also exhibits a broad band peaking at 375 nm with a shoulder at 308 nm. These two pairs of PL and PLE spectra at different wavelengths indicate that there are two types of Bi^{3+} emission centers in GGO hosts, which are attributed to the two different substitution sites of the Gd^{3+} ions according to the crystal structure. Therefore, the 409 and 594 nm PL peaks can originate from the $^3P_1$ excited state to the $^1S_0$ ground state transition of the Bi^{3+} ions located at the different sites, and the two peaks in the excitation spectrum can be attributed to the $^1S_0 \rightarrow {}^1P_1$ and $^1S_0 \rightarrow {}^3P_1$ transitions, respectively.[23–25] There are other reported mechanisms for the

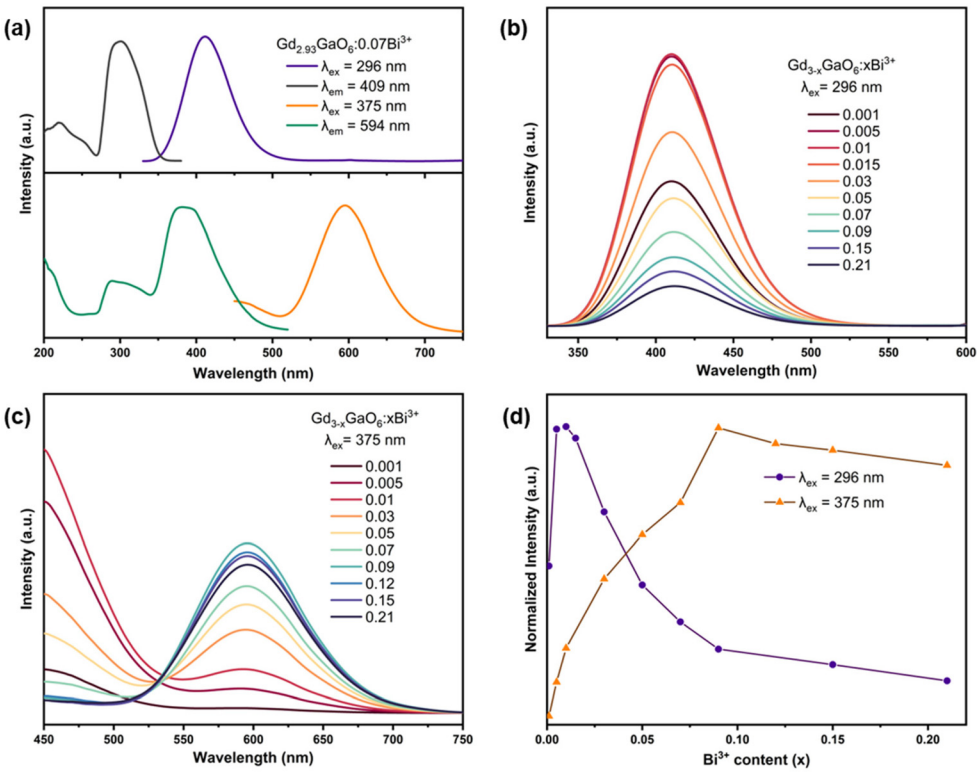

Fig. 2 (a) PL and PLE spectra of GGO:0.07Bi^{3+}. PL spectra of GGO:$x$$Bi^{3+}$ phosphors under 296 nm (b) and 375 nm (c) excitation. (d) The relative emission intensities of GGO:$x$$Bi^{3+}$ with various Bi^{3+} contents.

Bi^{3+} emission, namely emission from Bi^{3+} pairs and metal-to-metal charge transfer (MMCT). In some reported Bi^{3+}-doped phosphors with the Bi^{3+} pair emission mechanism,[26,27] the difference in excitation bands of the emissions is within 10 nm, which is much smaller than those of the emissions at 409 and 594 nm. Moreover, compared with the emission from MMCT,[28] the Stokes shift and bandwidth of the two emissions are much smaller. These observations substantiate that the emissions at 409 and 594 nm come from the different Bi^{3+} emission centers in different crystal sites.

In order to determine the cationic sites occupied by Bi^{3+}, it is necessary to determine the crystal field strength of both Gd1 and Gd2 sites. Generally, the crystal field splitting (D_q) can be estimated using the following equation:[29,30]

$$D_q = \frac{1}{6} Ze^2 \frac{r^4}{R^5} \quad (1)$$

where D_q denotes the magnitude of the 5d energy level separation, Z stands for the anion charge or valence, e is the electron charge, r represents the radius of the d wave function, and R is the bond length. On the basis of the above formula, the shorter the bond length, the stronger the crystal field splitting, resulting in a longer emission wavelength.[31,32] According to the bond length data of GGO:0.01Bi^{3+} (Table S2†), the average bond lengths (R) of Gd1–O and Gd2–O are 2.405 Å and 2.385 Å, respectively. Therefore, the emission peak at 409 nm should be assigned to the Bi^{3+} luminescent center located at Gd1 sites (denoted as Bi(I)) for the longer bond length, and the emission peak at 594 nm should be assigned to Bi^{3+} located at Gd2 sites (denoted as Bi(II)).

Fig. 2b shows the variation in PL spectra of Bi(I) in GGO:$x$$Bi^{3+}$ (x = 0.001–0.21) samples with increasing Bi^{3+} concentration under 296 nm excitation. The PL intensity increases as the concentration increases when $x < 0.01$, and then decreases due to the concentration quenching effect, which is caused by energy transfer between the neighboring Bi^{3+} ions. As for the Bi(II) luminescent center, Fig. 2c shows the PL intensity with various Bi^{3+} concentrations under 375 nm excitation. The emission intensity at 594 nm first increases, reaches a maximum at x = 0.09 and then begins to decrease. According to Fig. 2d, the emission peak at 594 nm gradually becomes dominant with the increasing concentration of Bi^{3+}. This indicates that the Bi^{3+} ions at low concentration occupy the Gd1 sites initially. As the concentration increases, they gradually enter the Gd2 sites. Additionally, there is an overlap between the PL spectra of Bi(I) and the PLE spectra of Bi(II), indicating the possibility of energy transfer from Bi(I) to Bi(II).

Fig. 3a shows the photoluminescence decay curves of Bi(II) and Bi(I) in GGO:0.07Bi^{3+}. Both of the curves can be fitted with a double exponential function using the following formula:[33,34]

$$I(t) = I_0 + A_1 \exp\left(-\frac{t}{\tau_1}\right) + A_2 \exp\left(-\frac{t}{\tau_2}\right) \quad (2)$$

where t is the time, $I(t)$ and I_0 are the luminescence intensities at time "t" and "0", A_1 and A_2 are constants, and τ_1 and τ_2 are the decay times of the exponential components, respectively. The values of A_1, A_2, τ_1 and τ_2 obtained by fitting are listed in Table 2. The average lifetime τ^* can be calculated using the following formula:[34,35]

$$\tau^* = \frac{A_1\tau_1^2 + A_2\tau_2^2}{A_1\tau_1 + A_2\tau_2}. \quad (3)$$

According to the above two formulas, the lifetime of Bi(II) emission is calculated to be τ^* = 1.32 μs, and the lifetime of Bi(I) is τ^* = 0.19 μs. It can be seen that the luminescence of Bi(I) decays faster than that of Bi(II), which further indicates that there can be the process of energy transfer from Bi(I) to Bi(II).

In addition, to investigate the effect of temperature on the luminescence properties, the PL spectra of GGO:0.01Bi^{3+} and GGO:0.09Bi^{3+} were measured in the temperature range of

Table 2 The values of A_1, A_2, τ_1, τ_2 and τ^*

Luminescent center	A_1	τ_1 (μs)	A_2	τ_2 (μs)	τ^* (μs)
Bi(I)	2178.21	0.051	2499.28	0.219	0.190
Bi(II)	3195.41	0.078	3025.24	1.392	1.319

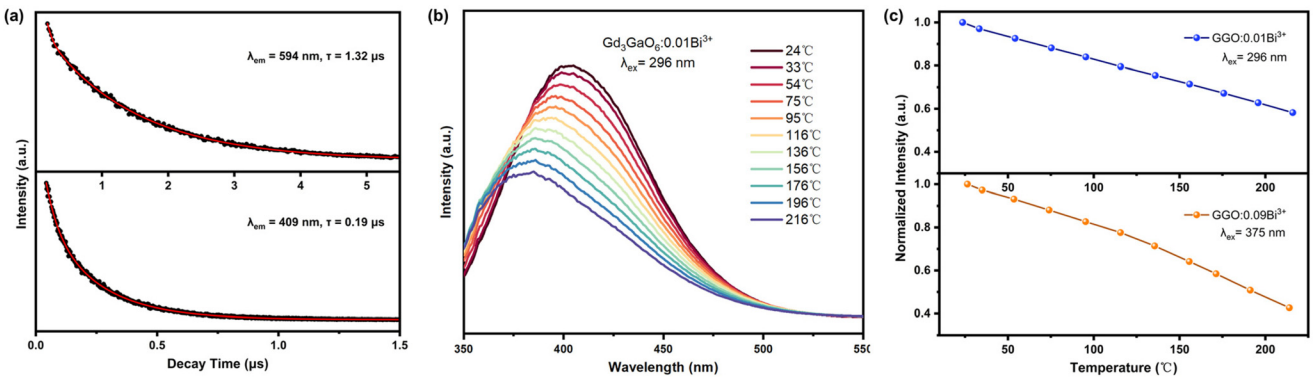

Fig. 3 (a) The photoluminescence decay curves of GGO:0.07Bi^{3+} monitored at 594 and 409 nm. (b) The temperature-dependent PL spectra of GGO:0.01Bi^{3+}. (c) PL intensity of GGO:0.01Bi^{3+} and GGO:0.09Bi^{3+} at different temperatures.

20–220 °C, as shown in Fig. 3b and S3.† It is clear that the emission intensity decreases with increasing temperature due to the thermal quenching effect, and the slight blue-shift can be ascribed to the thermally active phonon-assisted tunneling.[36,37] When the temperature reached 150 °C, the PL intensity at 409 nm of Bi(I) and the PL intensity at 594 nm of Bi(II) centers remained at 71% and 64% of that at room temperature, respectively (Fig. 3c). The high thermal stability is particularly valuable for the emission of Bi^{3+} with a large Stokes shift.[38] The linear curve of activation energy (Fig. S4†) and the coordinate diagram of thermal quenching (Fig. S5†) are further discussed and demonstrated in the ESI.†

3.3. Photoluminescence of GGO:Er^{3+} phosphors

Under the excitation at 378 nm, DS green luminescence can be observed in the single doped GGO:0.04Er^{3+} sample, as shown in the top panel of Fig. S6.† The PL spectrum mainly consists of two peaks at 527 and 549 nm, which are attributed to the $^2H_{11/2} \rightarrow {}^4I_{15/2}$ and $^3S_{3/2} \rightarrow {}^4I_{15/2}$ transitions of the Er^{3+} ions, respectively.[39,40] The excitation spectrum monitored at 549 nm was measured as shown in the bottom panel of Fig. S6,† which shows the best excitation at 376 nm from the $^4I_{15/2} \rightarrow {}^4G_{11/2}$ transition.

In addition to the above DS luminescence, the GGO:Er^{3+} sample can also exhibit characteristic UC luminescence. Fig. 4 shows the UC PL spectra of GGO:0.02Er^{3+} under different NIR excitation wavelengths (980 nm or 1530 nm). Both of the spectra exhibit two green bands peaking at about 535 and 549 nm, and a red emission band covering the range from 645 to 695 nm. These bands are assigned to the $^2H_{11/2} \rightarrow {}^4I_{15/2}$ (535 nm), $^4S_{3/2} \rightarrow {}^4I_{15/2}$ (549 nm) and $^4F_{9/2} \rightarrow {}^4I_{15/2}$ (645–695 nm) transitions of the Er^{3+} ions, respectively.[41,42] The corresponding UC luminescence mechanisms are demonstrated in Fig. 5. Furthermore, the UC PL spectra of different concentrations of GGO:yEr^{3+} (y = 0.02–0.08) are shown in Fig. S7.†

3.4. Photoluminescence of GGO:Bi^{3+},Er^{3+} phosphors

Fig. 6 shows the PL spectra of GGO:0.05Bi^{3+},0.04Er^{3+} under different excitation wavelengths. Under 296 nm excitation, it can be seen that the Bi(I) luminescent center still emits violet light at 409 nm and the Er^{3+} ions produce a weak emission at 550 nm (Fig. 6a). When excited at 375 nm, the Bi(II) luminescent center also exhibits orange light at around 600 nm and Er^{3+} shows strong emission at about 550 nm (Fig. 6b). Under 980 nm excitation, only Er^{3+} displays UC luminescence (Fig. S8†). These results indicate that the codoping with Bi^{3+} and Er^{3+} does not affect their original luminescence properties.

3.5. Anti-counterfeiting applications

On the basis of the unique multi-mode luminescence properties, the GGO:Bi^{3+}/Er^{3+} phosphors can be applied in anti-

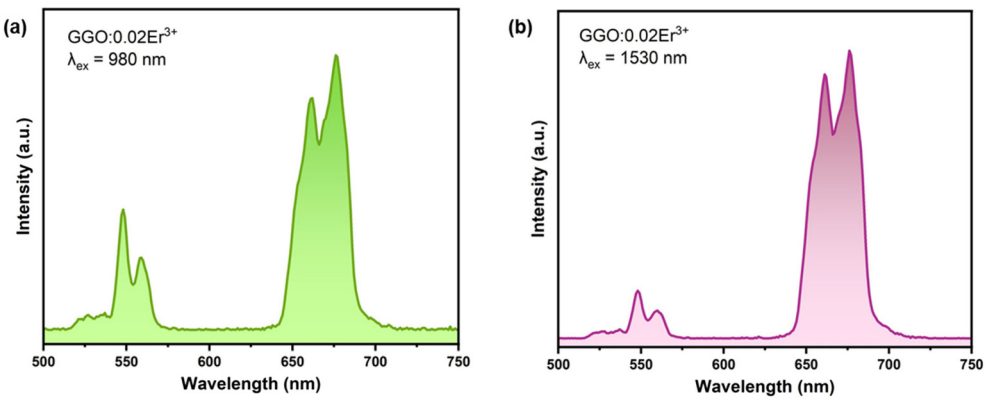

Fig. 4 The UC PL spectra of the GGO:Er^{3+} phosphor under (a) 980 nm and (b) 1530 nm.

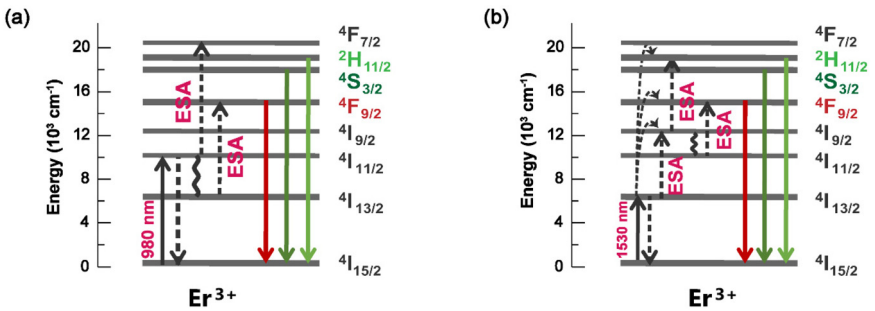

Fig. 5 Energy level diagrams and the UC process of the Er^{3+} ions under 980 nm (a) and 1530 nm (b) excitation.

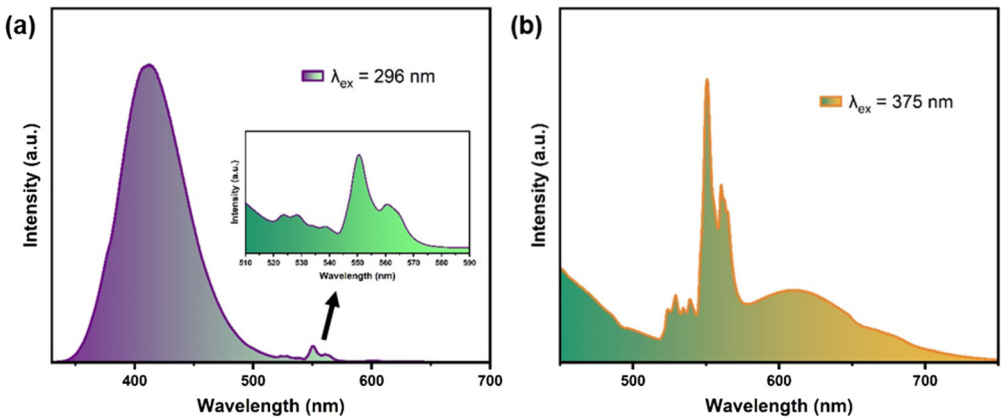

Fig. 6 PL spectra of GGO:0.05Bi^{3+},0.04Er^{3+} under the excitation of 296 (a) and 375 nm (b).

counterfeiting. As shown in Fig. 7a, GGO:0.05Bi^{3+}, GGO:0.07Bi^{3+},0.04Er^{3+} and GGO:0.04Er^{3+} are placed in a "GIA" glass mold and all the samples appear white in daylight. The "G" filled with the GGO:0.05Bi^{3+} phosphor displays clear blue-violet light and orange light when excited at 302 nm and 365 nm, respectively. However, there is no emission observed under 980 and 1530 nm excitation. On the other hand, the "A" filled with the GGO:0.04Er^{3+} phosphor does not emit any light under 302 nm excitation. However, it displays dark green, bright green, and yellow luminescence images under 365, 980, and 1530 nm excitation, respectively. The "I" filled with the GGO:0.07Bi^{3+},0.04Er^{3+} phosphor exhibits the same colors as "G" under 302 and 365 nm excitation. Interestingly, under 980 and 1530 nm excitation, it shows the corresponding images as observed with "A".

Moreover, by mixing the samples with transparent ink, the production of multi-mode anti-counterfeiting labels can be easily achieved. The simple diagram of the fabrication process is shown in Fig. 7b. As shown in Fig. 7c, the ink is mixed with GGO:0.07Bi^{3+},0.04Er^{3+} samples and a Chinese character "zhong" is written on the label paper. Interestingly, the character is hardly identifiable with the naked eye in daylight, but it exhibits clear and various colors under specific excitation wavelengths. It is worth mentioning that four distinguishable luminescence pictures can be obtained with just one phosphor under four different excitation wavelengths, which does not require a delicate core/shell structure,[7] a complicated lifetime measurement set-up,[13] or multiple kinds of similar phosphors.[8] These luminescent materials, which include both UC luminescence and DS luminescence, provide a high level of

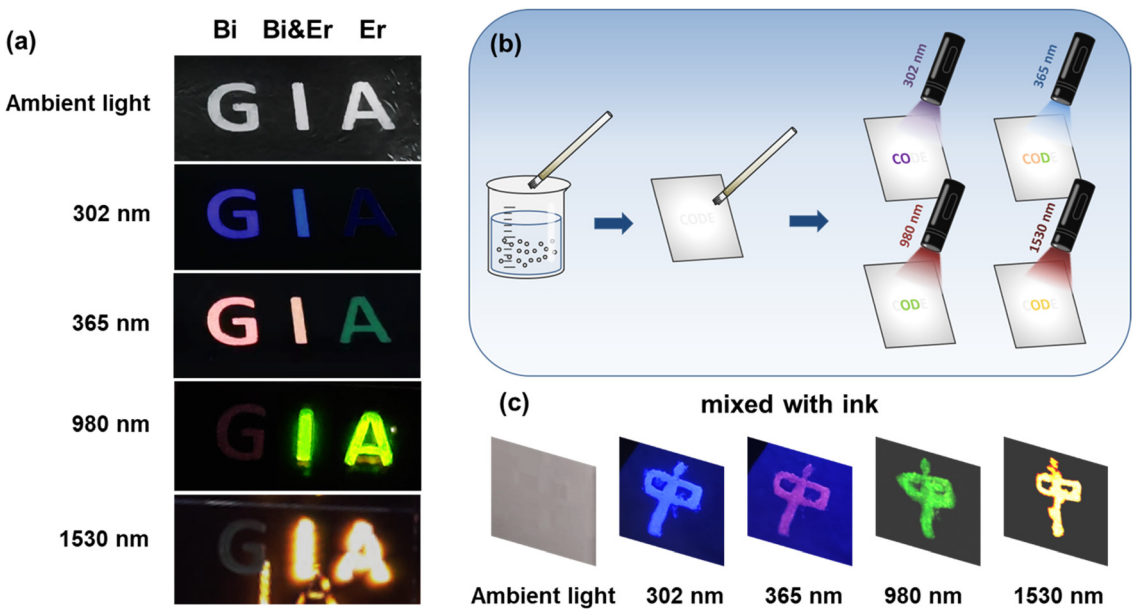

Fig. 7 (a) Digital photos of GGO:Bi/Er samples. (b) The manufacturing process and application diagram of the anti-counterfeiting label. (c) Demonstration of the anti-counterfeiting label by mixing the samples with transparent ink.

security and have the potential to further enhance the current anti-counterfeiting technology based on photoluminescence in society.

4. Conclusions

In summary, we have successfully synthesized the gallium oxide phosphors Gd_3GaO_6:Bi^{3+}/Er^{3+} with UC and DS luminescence by conventional high temperature solid state reactions. Rietveld refinement results indicate that the GGO matrix crystallized in the orthorhombic system with the space group $Cmc2_1$ (no. 36). The doped Bi^{3+} ions occupy the Gd^{3+} sites and exhibit violet and orange emissions at 409 nm and 594 nm. The Er^{3+} ions emit green light under 370 nm excitation and exhibit UC luminescence under the NIR light excitation of 980 and 1530 nm. And the Bi^{3+} and Er^{3+} codoped GGO samples present excitation orthogonalized emission under varied wavelengths. On the basis of the multi-color luminescence properties, the prepared phosphors with four luminescence modes were used to fabricate anti-counterfeiting labels. Highly distinguishable luminescence images were obtained under the excitations of 302, 365, 980 and 1530 nm. The results demonstrate that the multicolor luminescence can be easily detected using portable UV lamps and NIR lasers. This unique feature is difficult to counterfeit and provides a high level of security in the field of anti-counterfeiting.

Conflicts of interest

There are no conflicts of interest to declare.

Acknowledgements

The authors thank Bing Wang for her help in measuring decay lifetimes. This work is financially supported by the National Key Research and Development Program (Grant No. 2022YFC2905201), the National Natural Science Foundation of China (Grant No. 52072363), and the Research Project of Ganjiang Innovation Academy, Chinese Academy of Sciences (E255C001).

References

1 X. Zhao, S. Chen, C. Ye, L. Li, Y. Hu, X. Wang and Y. Song, Triplet–triplet annihilation upconversion combined with afterglow phosphors for multi-dimensional anti-counterfeiting and encoding, *J. Mater. Chem. C*, 2022, **10**, 12853–12862.

2 P. Kumara, J. Dwivedia and B. K. Gupta, Highly-luminescent dual mode rare-earth nanorods assisted multi-stage excitable security ink for anti-counterfeiting applications, *J. Mater. Chem. C*, 2014, **2**, 10468–10475.

3 T. Si, Q. Zhu, T. Zhang, X. Sun and J.-G. Li, Co-Doping Mn^{2+}/Cr^{3+} in $ZnGa_2O_4$ to Fabricate Chameleon-Like Phosphors for Multi-Mode Dynamic Anti-Counterfeiting, *Chem. Eng. J.*, 2021, **426**, 131744.

4 J. Zhang, Z. Wang, X. Huo, Y. Wang and P. Li, Multimodal dynamic color-tunable persistent luminescent phosphor $Ca_3Al_2Ge_3O_{12}$:Mn^{2+},Cr^{3+} for anti-counterfeiting and industrial inspection, *Inorg. Chem. Front.*, 2022, **9**, 6517–6526.

5 R. Arppe and T. J. Sorensen, Physical unclonable functions generated through chemical methods for anti-counterfeiting, *Nat. Rev. Chem.*, 2017, **1**, 0031.

6 X. Zhang, R. F. Ali, J. C. Boyer, N. R. Branda and B. D. Gates, Direct Photolithographic Deposition of Color–Coded Anti–Counterfeit Patterns with Titania Encapsulated Upconverting Nanoparticles, *Adv. Opt. Mater.*, 2020, **8**, 2000664.

7 H. Dong, L. D. Sun, W. Feng, Y. Gu, F. Li and C. H. Yan, Versatile Spectral and Lifetime Multiplexing Nanoplatform with Excitation Orthogonalized Upconversion Luminescence, *ACS Nano*, 2017, **11**, 3289–3297.

8 C. Zhuo, Z. Lyu, D. Sun, S. Shen, T. Tan, S. Wei, Z. Li, P. Luo and H. You, Lanthanide-doped Na_2MgScF_7 exhibiting downshifting and upconversion emissions for multicolor anti-counterfeiting, *Dalton Trans.*, 2023, **52**, 7322–7329.

9 Y. Zhang, L. Zhang, R. Deng, J. Tian, Y. Zong, D. Jin and X. Liu, Multicolor barcoding in a single upconversion crystal, *J. Am. Chem. Soc.*, 2014, **136**, 4893–4896.

10 Z. Y. Lyu, H. Dong, X. F. Yang, L. Huang, Y. J. Xu, K. Wu, L. D. Sun and C. H. Yan, Phase-Transition-Driven Regional Distribution of Rare-Earth Ions for Multiplexed Upconversion Emissions, *JACS Au*, 2023, **3**, 860–867.

11 S. Xie, G. Gong, Y. Song, H. Tan, C. Zhang, N. Li, Y. Zhang, L. Xu, J. Xu and J. Zheng, Design of novel lanthanide-doped core-shell nanocrystals with dual up-conversion and down-conversion luminescence for anti-counterfeiting printing, *Dalton Trans.*, 2019, **48**, 6971–6983.

12 W. Ren, G. Lin, C. Clarke, J. Zhou and D. Jin, Optical Nanomaterials and Enabling Technologies for High-Security-Level Anticounterfeiting, *Adv. Mater.*, 2020, **32**, 1901430.

13 Y. Lu, J. Zhao, R. Zhang, Y. Liu, D. Liu, E. M. Goldys, X. Yang, P. Xi, A. Sunna, J. Lu, Y. Shi, R. C. Leif, Y. Huo, J. Shen, J. A. Piper, J. P. Robinson and D. Jin, Tunable lifetime multiplexing using luminescent nanocrystals, *Nat. Photonics*, 2013, **8**, 32–36.

14 Z. Li, Z. Lyu, D. Sun, S. Shen and H. You, The downshifting and upconversion photoluminescence from $NaBaSc_2(PO_4)_3$ for multicolor anti-counterfeiting, *Mater. Today Chem.*, 2022, **26**, 101116.

15 B. Zhang, S. Ying, S. Wang, L. Han, J. Zhang and B. Chen, Blue-Green-Yellow Color-Tunable Luminescence of Ce^{3+}-, Tb^{3+}-, and Mn^{2+}-Codoped $Sr_3YNa(PO_4)_3F$ via Efficient Energy Transfer, *Inorg. Chem.*, 2019, **58**, 4500–4507.

16 Y. L. Yang, X. C. Yang, J. Y. Yuan, T. Li, Y. T. Fan, L. Wang, Z. Deng, Q. L. Li, D. Y. Wan, J. T. Zhao and Z. J. Zhang, Time–Resolved Bright Red to Cyan Color Tunable

Mechanoluminescence from CaZnOS:Bi^{3+},Mn^{2+} for Anti–Counterfeiting Device and Stress Sensor, *Adv. Opt. Mater.*, 2021, **9**, 2100668.

17 S. Miao, Y. Liang, D. Chen, S. Yan, J. Liu, W. Wang and J. Bi, Enabling narrowband cyan photoluminescence and long-lasting ultraviolet-A persistent luminescence in Bi^{3+} single-doped $Sr_3Sc_2Ge_3O_{12}$ phosphors by selective site occupation, *J. Mater. Chem. C*, 2022, **10**, 14211–14219.

18 K. Li, J. Fan, M. Shang, H. Lian and J. Lin, $Sr_2Y_8(SiO_4)_6O_2$:Bi^{3+}/Eu^{3+}: a single-component white-emitting phosphor via energy transfer for UV w-LEDs, *J. Mater. Chem. C*, 2015, **3**, 9989–9998.

19 X. Wang, J. Wang, X. Li, H. Luo and M. Peng, Novel bismuth activated blue-emitting phosphor $Ba_2Y_5B_5O_{17}$:Bi^{3+} with strong NUV excitation for WLEDs, *J. Mater. Chem. C*, 2019, **7**, 11227–11233.

20 H. Huang, J. Chen, Y. Liu, J. Lin, S. Wang, F. Huang and D. Chen, Lanthanide-Doped Core@Multishell Nanoarchitectures: Multimodal Excitable Upconverting/Downshifting Luminescence and High-Level Anti-Counterfeiting, *Small*, 2020, **16**, 2000708.

21 X. Fan, J. Nie, W. Ying, S. Xu, J. Gu and S. Liu, Cryogenic enabled multicolor upconversion luminescence of KLa$(MoO_4)_2$:Yb^{3+}/Ho^{3+} for dual-mode anti-counterfeiting, *Dalton Trans.*, 2021, **50**, 12234–12241.

22 G. Chen, H. Agren, T. Y. Ohulchanskyy and P. N. Prasad, Light upconverting core-shell nanostructures: nanophotonic control for emerging applications, *Chem. Soc. Rev.*, 2015, **44**, 1680–1713.

23 Y. Wang, N. Guo, B. Shao, C. Yao, R. Ouyang and Y. Miao, Adjustable Photoluminescence of Bi^{3+} and Eu^{3+} in Solid Solution Constructed by Isostructural End Components through Composition and Excitation-Driven Strategy, *Chem. Eng. J.*, 2021, **421**, 127735.

24 K. Li, H. Lian, M. Shang and J. Lin, A Novel Greenish Yellow-Orange Red $Ba_3Y_4O_9$:Bi^{3+},Eu^{3+} Phosphor with Efficient Energy Transfer for UV-LEDs, *Dalton Trans.*, 2015, **44**, 20542–20550.

25 P. Dang, S. Liang, G. Li, Y. Wei, Z. Cheng, H. Lian, M. Shang, S. J. Ho and J. Lin, Controllable Optical Tuning and Improvement in Li^+,Eu^{3+}-Codoped $BaSc_2O_4$:Bi^{3+} Based on Energy Transfer and Charge Compensation, *J. Mater. Chem. C*, 2018, **6**, 6449–6459.

26 A. M. Srivastava, On the luminescence of Bi^{3+} in the pyrochlore $Y_2Sn_2O_7$, *Mater. Res. Bull.*, 2002, **37**, 745–751.

27 A. A. Setlur and A. M. Srivastava, The nature of Bi^{3+} luminescence in garnet hosts, *Opt. Mater.*, 2006, **29**, 410–415.

28 S. Ye, J. Ding and Q. Wu, MMCT-induced high-bright yellow light-emitting phosphor Bi^{3+}-activated Ba_2YGaO_5 used for WLED, *Chem. Eng. J.*, 2022, **428**, 131238.

29 Y. Tian, Y. Wei, Y. Zhao, Z. Quan, G. Li and J. Lin, Photoluminescence Tuning of $Ca_5(PO_4)_3Cl$:Ce^{3+}/Eu^{2+},Tb^{3+}/Mn^{2+} Phosphors: Structure Refinement, Site Occupancy, Energy Transfer and Thermal Stability, *J. Mater. Chem. C*, 2016, **4**, 1281–1294.

30 D. Zhang, X. Zhang, B. Zheng, Q. Sun, Z. Zheng, Z. Shi, Y. Song and H. Zou, Li^+ Ion Induced Full Visible Emission in Single Eu^{2+}–Doped White Emitting Phosphor: Eu^{2+} Site Preference Analysis, Luminescence Properties, and WLED Applications, *Adv. Opt. Mater.*, 2021, **9**, 2100337.

31 P. Dorenbos, Energy of the First $4f^7 \rightarrow 4f^6 5^d$ Transition of Eu^{2+} in Inorganic Compounds, *J. Lumin.*, 2003, **104**, 239–260.

32 G. Li, Y. Tian, Y. Zhao and J. Lin, Recent Progress in Luminescence Tuning of Ce^{3+} and Eu^{2+}-Activated Phosphors for pc-WLEDs, *Chem. Soc. Rev.*, 2015, **44**, 8688–8713.

33 B. Yu, Y. Li, Y. Wang and L. Geng, Double-Site Eu^{3+} Occupation in the Langbeinite-Type Phosphate Phosphor toward Adjustable Emission for pc-WLEDs, *J. Alloys Compd.*, 2021, **874**, 159862.

34 B. Shao, J. Huo and H. You, Prevailing Strategies to Tune Emission Color of Lanthanide–Activated Phosphors for WLED Applications, *Adv. Opt. Mater.*, 2019, **7**, 1900319.

35 P. Dang, S. Liang, G. Li, H. Lian, M. Shang and J. Lin, Broad Color Tuning of Bi^{3+}/Eu^{3+}-Doped $(Ba,Sr)_3Sc_4O_9$ Solid Solution Compounds via Crystal Field Modulation and Energy Transfer, *J. Mater. Chem. C*, 2018, **6**, 9990–9999.

36 X. Liu, P. Xiong, H. Liu, S. Wu, Q. Liu, Y. Fu, Z. Ma, M. Peng and Q. Zhang, Origin of D-band emission in a novel Bi^{3+}-doped phosphor $La_3SnGa_5O_{14}$:Bi^{3+}, *J. Mater. Chem. C*, 2021, **9**, 3455–3461.

37 D. Wang, Z. Tang, W. U. Khan and Y. Wang, Photoluminescence study of a broad yellow-emitting phosphor $K_2ZrSi_2O_7$:Bi^{3+}, *Chem. Eng. J.*, 2017, **313**, 1082–1087.

38 H. Li, R. Pang, G. Liu, W. Sun, D. Li, L. Jiang, S. Zhang, C. Li, J. Feng and H. Zhang, Synthesis and Luminescence Properties of Bi^{3+}-Activated K_2MgGeO_4: A Promising High-Brightness Orange-Emitting Phosphor for WLEDs Conversion, *Inorg. Chem.*, 2018, **57**, 12303–12311.

39 W. Ran, H. M. Noh, S. H. Park, B. R. Lee, J. H. Kim, J. H. Jeong and J. Shi, Er^{3+}-Activated $NaLaMgWO_6$ Double Perovskite Phosphors and Their Bifunctional Application in Solid-State Lighting and Non-Contact Optical Thermometry, *Dalton Trans.*, 2019, **48**, 4405–4412.

40 P. Pei, R. Wei, B. Wang, J. Su, Z. Zhang and W. Liu, An Advanced Tunable Multimodal Luminescent La_4GeO_8:Eu^{2+}, Er^{3+} Phosphor for Multicolor Anticounterfeiting, *Adv. Funct. Mater.*, 2021, **31**, 2102479.

41 Y. Liu, Z. Zhou, S. Zhang, E. Zhao, J. Ren, L. Liu and J. Zhang, Mechanisms of Upconversion Luminescence of Er^{3+}-Doped $NaYF_4$ via 980 and 1530 nm Excitation, *Nanomaterials*, 2021, **11**, 2767.

42 R. Krishnan, G. B. Nair, S. G. Menon, L. Erasmus and H. C. Swart, Synthesis of Tm_2WO_6:Er^{3+} upconversion phosphor for high-contrast imaging of latent-fingerprints, *J. Alloys Compd.*, 2021, **878**, 160386.